Self-Targeting Fluorescent Carbon Dots for Diagnosis of Brain Cancer Cells

Min Zheng,[†,‡,§] Shaobo Ruan,[⊥] Shi Liu,[§] Tingting Sun,[§,#] Dan Qu,[‡,#] Haifeng Zhao,[‡] Zhigang Xie,[*,§] Huile Gao,[*,⊥] Xiabin Jing,[§] and Zaicheng Sun[*,‡,∥]

[†]Chemistry and Life Science School, Advanced Institute of Materials Science, Changchun University of Technology, 2055 Yanan Street, Changchun, Jilin 130012, People's Republic of China, [‡]State Key Laboratory of Luminescence and Applications, Changchun Institute of Optics, Fine Mechanics, and Physics, Chinese Academy of Sciences, 3888 East Nanhu Road, Changchun, Jilin 130033, People's Republic of China, [§]State Key Laboratory of Polymer Physics and Chemistry, Changchun Institute of Applied Chemistry, Chinese Academy of Sciences, 5625 Renmin Street, Changchun, Jilin 130022, People's Republic of China, [⊥]Key Laboratory of Drug Targeting and Drug Delivery Systems, West China School of Pharmacy, Sichuan University, No. 17 Block 3, Southern Renmin Road, Chengdu, 610041, People's Republic of China, [#]University of Chinese Academy of Sciences, Beijing 100049, People's Republic of China, and [∥]Beijing Key Laboratory for Green Catalysis and Separation, Department of Chemistry and Chemical Engineering, Beijing University of Technology, Beijing 100124, People's Republic of China

ABSTRACT A new type of carbon dots (CD-Asp) with targeting function toward brain cancer glioma was synthesized *via* a straightforward pyrolysis route by using D-glucose and L-aspartic acid as starting materials. The as-prepared CD-Asp exhibits not only excellent biocompatibility and tunable full-color emission, but also significant capability of targeting C6 glioma cells without the aid of any extra targeting molecules. *In vivo* fluorescence images showed high-contrast biodistribution of CD-Asp 15 min after tail vein injection. A much stronger fluorescent signal was detected in the glioma site than that in normal brain, indicating their ability to freely penetrate the blood–brain barrier and precisely targeting glioma tissue. However, its counterparts, the CDs synthesized from D-glucose (CD-G), L-asparic acid (CD-A), or D-glucose and L-glutamic acid (CD-Glu) have no or low selectivity for glioma. Therefore, CD-Asp could act as a fluorescence imaging and targeting agent for noninvasive glioma diagnosis. This work highlights the potential application of CDs for constructing an intelligent nanomedicine with integration of diagnostic, targeting, and therapeutic functions.

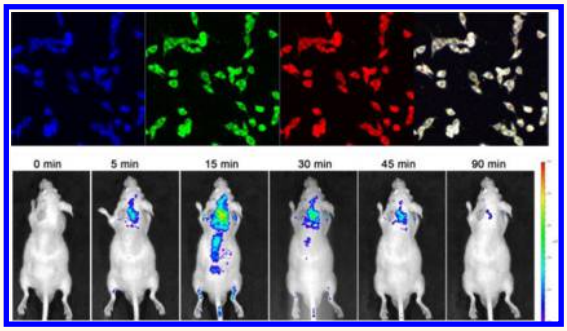

KEYWORDS: carbon dots · full-color emission · targeted imaging · brain cancer glioma · diagnosis

Central nervous system (CNS) tumors are a crucial cause of morbidity and mortality worldwide. Among them, gliomas are the most common and lethal primary brain tumor in humans.[1] Thus, accurately imaging the glioma cells is urgent for the early diagnosis and effective treatment of brain glioma. Recent research has witnessed that fluorescence imaging techniques are effectively used to detect tumor cells due to their numerous merits, for instance, high sensitivity, high contrast, and controllable targeting.[2] At present, the emergence of fluorescent semiconductor nanocrystals (quantum dots, QDs) opens a new avenue for fluorescence imaging technology due to their significant advantages such as tiny size, tunable color, and high photoluminescence quantum yield (PL QY).[3−7] However, the intrinsic toxicity of QDs severely limits their practical applications in biomedical fields.[4] An extra nontoxic shell (silica or PEG) is necessary to lower the toxicity. More important is that targeting molecules (transferrin antibody or receptor) need to be tied on the surface of QDs in order to concentrate the fluorescent agent in the tumor site and enhance the imaging contrast.[8−12] That is a burdensome process to obtain an excellent diagnosis agent to achieve an early diagnosis of tumor. Thus, it is highly desired to synthesize a nontoxic, highly biocompatible, and fluorescent agent combined with a targeting function in a simple route to achieve effective diagnosis of tumor even at an early stage.

Photoluminescent carbon dots (CDs) have attracted ever-increasing interest due

* Address correspondence to xiez@ciac.ac.cn (Z. Xie), gaohuile@scu.edu.cn (H. Gao), sunzc@bjut.edu.cn (Z. Sun).

Received for review September 4, 2015 and accepted October 12, 2015.

Published online October 12, 2015
10.1021/acsnano.5b05575

to their alluring properties such as excellent biocompatibility, water solubility, good cell membrane permeability, high photostability, and tunable surface functional groups.[13−20] Many reports have demonstrated that they can serve as nontoxic substitutes for traditional heavy-metal-based QDs.[21−25] Thus, CDs are good candidates for fluorescence bioimaging.[26−41] In our previous report, CDs were used as a bioimaging agent and universal scaffold attached with extra therapeutic agents for the personal customized nanomedicine.[42] However, tethering the targeting molecules onto the CDs still remains a great challenging for constructing a perfect "smart" theranostic agent, which is a multiple functional platform integrating imaging, targeting, and therapeutic functions.

In the present work, novel fluorescent CD-Asp with self-targeting ability were synthesized *via* a simple thermolysis route by using D-glucose and L-aspartic acid as starting materials. The as-prepared CD-Asp not only exhibit tunable full-color emission but also show high selectivity and enrichment in brain C6 glioma cells without the aid of any extra targeting molecules. When CD-Asp were injected through the mouse tail vein, *in vivo* fluorescence images showed high contrast biodistribution of CD-Asp 15 min after injection. This indicates that CD-Asp have both bioimaging and targeting functions toward C6 glioma cells *in vitro*. A much stronger fluorescent signal was detected in the glioma site than that in normal brain, further confirming their ability to freely penetrate the blood−brain barrier (BBB) and precisely target glioma tissue. By contrast, other kinds of CDs (CD-G, CD-A, and CD-Glu) exhibit no or low selectivity for gliomas. This work demonstrates that CD-Asp could act as a fluorescence imaging and targeting agent for noninvasive glioma diagnosis.

RESULTS AND DISCUSSION

As is typical, CD-Asp was prepared with an equal molar mixture of D-glucose and L-aspartic acid (L-Asp) in a 1.0 mol/L NaOH aqueous solution at 200 °C for 20 min (see the Supporting Information for the detailed preparation process). The as-prepared CD-Asp dispersion remains clear and homogeneous at room temperature over a few months. Figure 1a shows the transmission electron microscopy (TEM) images of CD-Asp, which were drop-cast from the water dispersion on a carbon-coated copper grid. The images show that CD-Asp has a uniform diameter of 2.28 ± 0.42 nm (Figure 1A). High-resolution TEM (HR-TEM) images illustrate that most CD-Asp have well-resolved lattice structures with a *d* spacing value of 0.21 nm (Figure 1B and C), in agreement with the basal spacing of graphite. The fast Fourier transform (FFT) pattern of the representative CD-Asp is inset in the corresponding HR-TEM image (Figure 1D), and the observed hexagonal lattice in the FFT images reveals that the CD-Asp are crystalline hexagonal structures. The X-ray diffraction (XRD) patterns of the CD-Asp were obtained to identify their crystalline nature, as shown in Figure S1; two broad diffraction peaks centered at 2θ = 29.7° and 42.2°, showing *d* spacings of 0.30 and 0.21 nm, respectively, are attributed to the graphite lattice spacings of (002) and (100). This further confirms the crystalline graphite-like structure of as-prepared CD-Asp. Atomic force microscopy (AFM) images (Figure 1E) show that the as-prepared CD-Asp can highly disperse in water and remain as individual particles. The height profile along the line cut reveals that the height of CD-Asp is 0.4 to 1.4 nm, suggesting that there are 1−4 layers of graphene sheets based on 0.34 nm of single-layer graphene thickness.

The full-scan X-ray photoelectron spectroscopy (XPS) spectrum of CD-Asp is shown in Figure S2. Three peaks at 284.6, 399.4, and 530.9 eV are attributed to C 1s, N 1s, and O 1s XPS characteristic peaks, respectively. The ratio of N/C is 0.03, indicating a small amount of N atoms are doped into CD-Asp. The high-resolution XPS spectra of C 1s (Figure 2A) can be well deconvolved into three components, corresponding to sp^2 C atoms in C═C/C−C at a binding energy of 284.6 eV, sp^3 carbons in C−N/C−O at 285.9 eV, and a carboxyl group (CO_2H) at 288.6 eV. The high-resolution N 1s XPS spectra of CD-Asp (Figure 2B) reveal the presence of secondary amine (399.5 eV) and pyrrolic N (400.2 eV) atoms, further confirming the incorporation of N atoms in CD-Asp. Fourier transform infrared (FT-IR) spectra were used to identify the surface functional groups present on the CD-Asp surface. As shown in Figure S3, the vibration bands at 1389, 1582, and 3383 cm^{-1} demonstrated the presence of the respective aromatic amine and the aromatic skeleton of C═C, hydroxyl, and carboxyl groups, respectively. A negative zeta potential (Table S1, −22.8 mV) of the CD-Asp was recorded in aqueous solution, corroborating the presence of a lot of carboxylic groups on their surface. The hydrophilic groups facilitate dispersing of CD-Asp in aqueous solution. Two wide absorption bands at 277 and 332 nm were observed in the UV−vis absorption spectrum (Figure S4) of CD-Asp, which originated from the $\pi-\pi^*$ transition of multiple polyaromatic chromophores and the $n-\pi^*$ transition of carbonyl groups, respectively. It is worth mentioning that CD-Asp exhibit concentration-dependent luminescence behaviors; at a concentration of 0.02 mg/mL, the maximum PL intensity was observed under an excitation of 380 nm (Figure 2D) with the absolute fluorescence quantum yield of 7.5%, and with an increase in the concentration from 0.1 mg/mL to 0.4 mg/mL, the maximum excitation wavelength is red-shifted from 380 nm to 460 nm (Figure S5, Figure 2C and D), with the highest emission wavelength shifting from 465 nm to 550 nm. The longer excitation/emission wavelength could endow CD-Asp with the ability to be detected when they

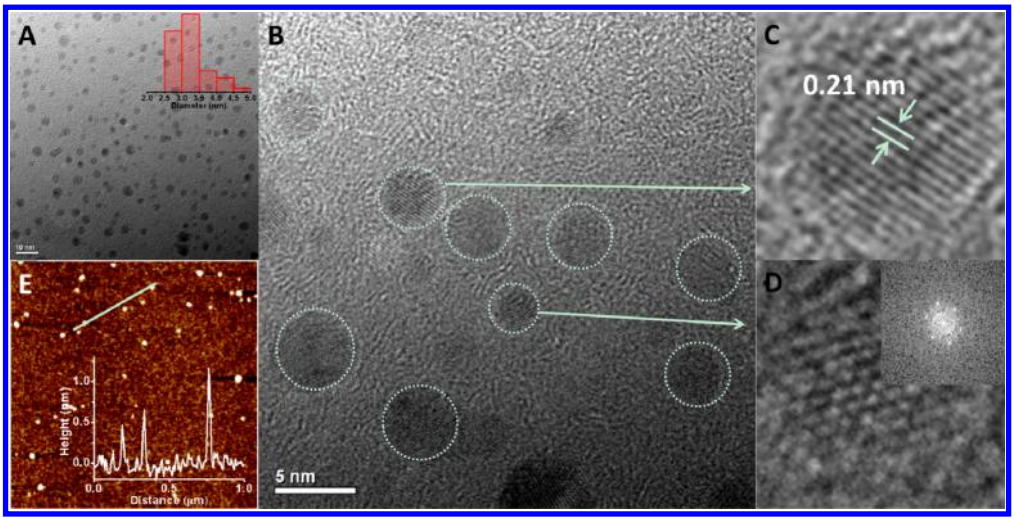

Figure 1. (A) Transmission electron microscopy (TEM) images of CD-Asp. The inset image is the diameter distribution of CD-Asp. (B) High-resolution TEM image of CD-Asp. (C and D) Highlighted areas of B. The inset in D is the fast Fourier transform pattern, which shows crystalline hexagonal structures of CD-Asp. (E) AFM image of CD-Asp. The inset is the height profile along the line in E.

penetrate into deeper tissues. Moreover, the excitation-dependent feature was found for each concentration of CD-Asp, which is similar to those of previously reported carbon nanoparticles.[43−45] Taking 0.2 mg/mL of CD-Asp as an example, the emission band shifts from 475 nm to 635 nm with an increase of excitation wavelength from 340 nm to 600 nm (Figure S5D); the gorgeous characteristics of continuous excitation-dependent full-color emission endows CD-Asp with optical bioimaging ability.

The cytotoxicity of CD-Asp was measured to make sure that as-synthesized CD-Asp possess low cytotoxicity and are suitable for biological applications. Cellular biocompatibility experiments were conducted by using the MTT method with C6 glioma and noncancerous cells (L929 mouse fibroblast cells) as test cell lines. As shown in Figure S6A, in contrast with the control group, all of the survival rates of the cells exceed ~75% after incubation with CD-Asp for 48 h at six different concentrations (10 to 500 μg/mL). These results indicate that CD-Asp do not obviously inhibit the proliferation of the cells, confirming that CD-Asp are suitable for biomedical applications. Laser confocal scanning microscopy (LCSM) was used to further demonstrate the biomedical applications of CD-Asp, and the *in vitro* cell imaging of CD-Asp is shown in Figure S6B−E. After incubation with CD-Asp for 1 h, the cell-internalized CD-Asp can emit intense blue, green, and red colors under excitation at 405, 488, and 555 nm, respectively. CD-Asp can label the areas of membrane and cytoplasm of C6 cells without photobleaching, as observed in the LCSM study. The good biocompatibility, broad tunability, and remarkably high photostability are extremely beneficial for bioimaging and detection.

To demonstrate the selectivity of CD-Asp toward C6 cells, LCSM imaging was conducted on C6 and L929

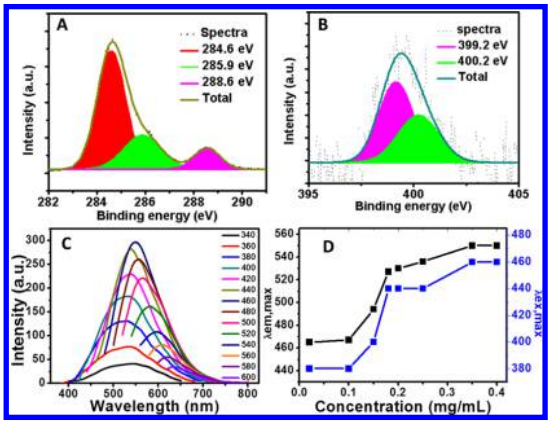

Figure 2. (A) High-resolution C 1s XPS. (B) High-resolution N 1s XPS spectra of the CD-Asp. (C) Photoluminescent spectra of CD-Asp (0.35 mg/mL) under different excitation wavelengths. (D) Dependence of the maximum excitation wavelengths and maximum emission wavelengths on the concentration of CD-Asp.

cells that were cultivated with 2 mg/mL of CD-Asp for 1 h, respectively. As shown in Figure 3A−C and E−G, the mean fluorescence intensity of C6 cells is much stronger than that of L929 cells, indicating more uptake of CD-Asp by C6 cells than that by noncancerous L929 cells and the selectivity of CD-Asp toward cancerous C6 cells. In order to further quantify CD-Asp selectivity on each cell line, flow cytometry was used to measure the fluorescence intensities of C6 and L929 cells treated with CD-Asp. As shown in Figure 3D and H, the endocytosis rate of CD-Asp in C6 and L929 cells is 72.5% and 34%, respectively, in agreement with the LCSM results and further confirming the high selectivity of CD-Asp toward C6 cells. Therefore, CD-Asp can serve as a promising highly fluorescent imaging agent with promising targeting properties on C6 glioma cells.

In order to investigate the selectivity of CD-Asp toward C6 cells, the internalization of CD-Asp by C6 and L929 cells was carried out at 37 and 4 °C, respectively. As shown in Figure 3I–M, upon incubation with CD-Asp at 37 °C for 1 h, the C6 cells became bright green under excitation at 488 nm (mean fluorescence intensity: 226.0); however, relatively faint fluorescence (mean fluorescence intensity: 81.5) was observed in the case of C6 cells incubated with CD-Asp at 4 °C (Figure 3I and J), indicating that CD-Asp were mainly taken up by C6 cells through energy-dependent endocytosis, which is consistent with the previous work.[46] However, the mean fluorescence intensity difference of the L929 cell line between 37 °C (76.2) and 4 °C (63.7) was not statistically significant (Figure 3K and L), which means that a greater fraction of CD-Asp is translocated into L929 cells *via* a passive transport process, which requires less energy. Furthermore, in order to investigate possible factors that determine the selectivity of CD-Asp toward C6 cells, the CDs were synthesized from D-glucose (CD-G, Figure S7) and L-Asp (CD-A, Figure S8) individually, instead of their 1:1 mixture, and the uptake of CD-G and CD-A by C6 and L929 cells was conducted under the same conditions as used for CD-Asp. Consequently, almost no difference between C6 and L929 cells was observed (Figure S9A–D), indicating that these CDs do not have a targeting ability toward C6 cells. L-Glutamic acid (L-Glu), which differs from L-Asp in just one methyl group, along with glucose, was used to prepare CD-Glu (see Supporting Information, Figure S10) in the same conditions, and the uptake of CD-Glu by C6 and L929 cells was conducted. No difference was found between C6 and L929 cells (Figure S9E and F). This result indicates that CD-Glu do not show the ability of targeting C6 cells either. Although glutamic acid and L-Asp differ by only one methyl group, the CDs made from them gave distinct results.

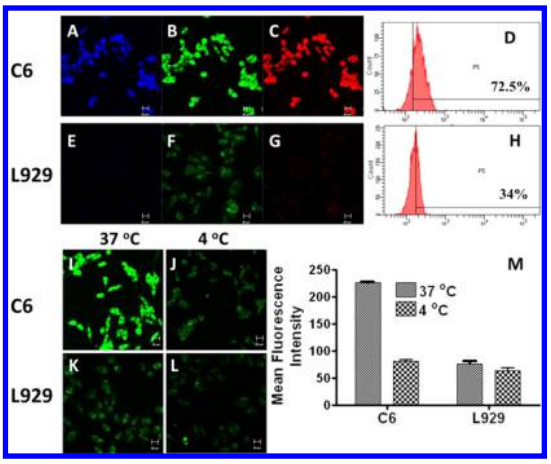

Figure 3. LSCM images of C6 (A–C) and L929 (E–G) cell lines pretreated with CD-Asp for 1 h at 37 °C, under excitation of 405, 488, and 555 nm. The scale bar is 20 μm. Flow cytometric profiles of C6 (D) and L929 (H) cells treated with CD-Asp for 1 h. LCSM images of C6 cells labeled with CD-Asp at 37 °C (I) and 4 °C (J) and L929 cells labeled with CD-Asp at 37 °C (K) and 4 °C (L) under 488 nm excitation, respectively. The scale bar is 20 μm. (M) mean fluorescence intensities of I, J, K, and L were calculated using Image-Pro Plus 6.0 software.

In vivo imaging of orthotopic C6 glioma-bearing mice was conducted by using an *in vivo* imaging system (IVIS Spectrum, Caliper, USA). As shown in Figure 4A, CD-Asp could accumulate in the brain site 5 min after the injection from the tail vein, indicating that CD-Asp could easily pass through the BBB and reach the brain tissue. The highest fluorescent intensity was observed at 15 min and then decreased gradually with increasing time, indicating that CD-Asp could enrich at the glioma with systemic elimination. Three dimensional (3D) reconstruction imaging was performed

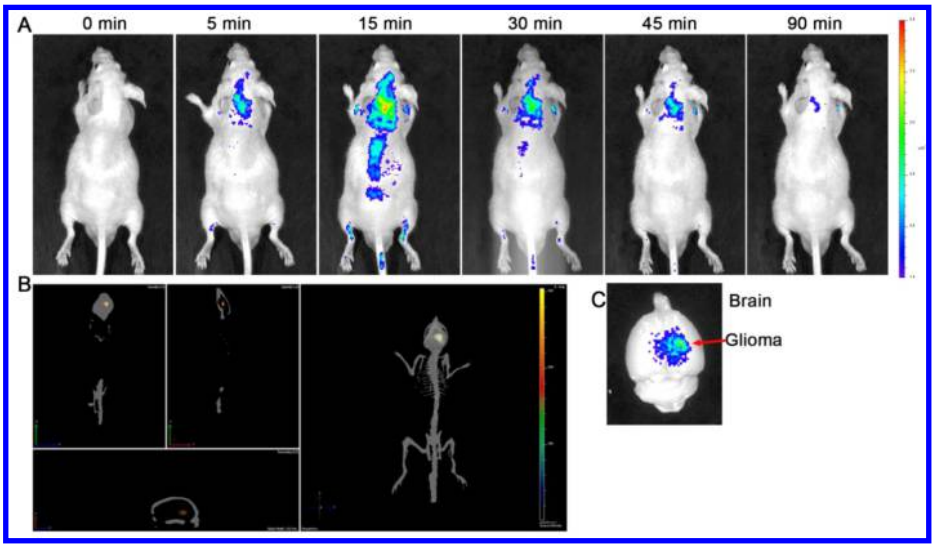

Figure 4. *In vivo* and *ex vivo* imaging of glioma-bearing mice after tail intravenous injection of CD-Asp. (A) Whole body distribution of CD-Asp as a function of time after injection. (B) Three-dimensional reconstruction of CD-Asp distribution in the brain 20 min after injection. (C) *Ex vivo* imaging of the brain 90 min after the injection of CD-Asp.

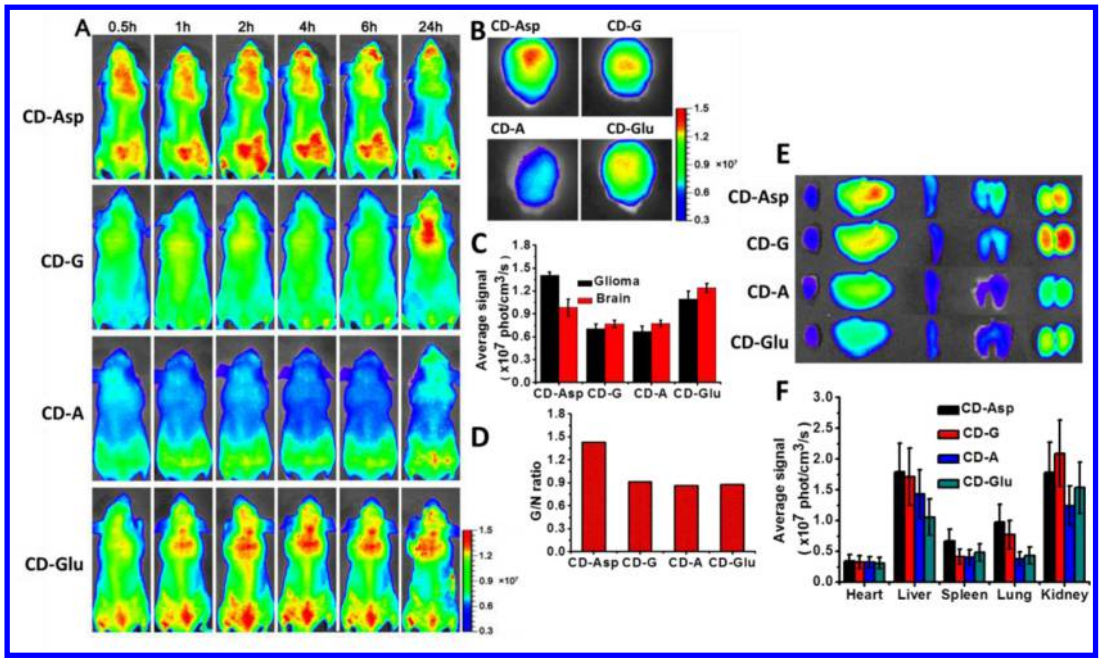

Figure 5. *In vivo* **and** *ex vivo* **imaging of CD-Asp, CD-G, CD-A, and CD-Glu treated glioma-bearing mice. (A)** *In vivo* **imaging of glioma-bearing mice at different time points after injection with CD-Asp, CD-G, CD-A, and CD-Glu. (B)** *Ex vivo* **imaging of glioma-bearing brain. (C) Semiquantitative fluorescent intensity of brain and glioma. (D) G/N ratio of CD-Asp, CD-G, CD-A, and CD-Glu groups. (E)** *Ex vivo* **imaging of normal tissues 24 h after the injection of CD-Asp, CD-G, CD-A, and CD-Glu. (F) Semiquantitative fluorescent intensity of heart, liver, spleen, lung, and kidney.**

20 min after injection; the result (Figure 4B) showed the fluorescent intensity in the glioma site was much stronger than that in normal brain issue, confirming that CD-Asp could localize in the glioma site. In addition, *ex vivo* imaging (Figure 4C) of the brain further confirms that CD-Asp target on the glioma site. For comparison, CD-Asp, CD-G, CD-A, and CD-Glu were intravenously (i.v.) injected into mice through the tail vein at an equivalent dose of 200 mg/kg, respectively. Then the fluorescent distribution in the whole body was detected through an *in vivo* imaging system at different time points: 0.5, 1, 2, 4, 6, and 24 h. As shown in Figure 5A, B, and C, although CD-Asp, CD-G, CD-A, and CD-Glu could distribute into the brain site, the intensity of mice injected with CD-Asp was much higher than that of the other three groups. The glioma/normal brain ratio (G/N ratio) (Figure 5D) was used to directly compare the glioma targeting efficiency of CD-Asp, CD-G, CD-A, and CD-Glu. The G/N ratio for CD-Asp, CD-G, CD-A, and CD-Glu group is 1.42, 0.91, 0.86, and 0.88, indicating that only CD-Asp exhibit obvious glioma-targeting efficiency. These results are consistent with the previous LSCM experiments. Taking targeting selectivity of CD-Asp toward C6 cells into consideration, it is deduced that the CD-Asp can target glioma sites and act as a fluorescence imaging agent for glioma diagnosis. The fluorescence intensities of normal organs (Figure 5E) follow the order kidney > liver > lung > spleen > heart. There was no obvious difference among CD-Asp, CD-G, and CD-A in the distribution in normal tissues, indicating that the targeting function of CD-Asp did not elevate the distribution of CDs in the normal tissues.

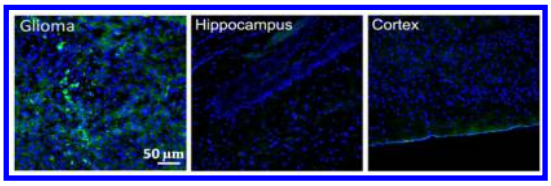

Figure 6. Distribution of CD-Asp in glioma, the hippocampus, and the cortical layer 24 h after injection. Green represents CD-Asp; blue represents nuclei.

In order to further elucidate the distribution of CD-Asp in different tissues, tissue slices were prepared and subjected to fluorescence microscopy. As shown in Figure 6, CD-Asp displayed much higher localization in glioma than that in the cortical layer and hippocampus of the brain, indicating CD-Asp could target glioma rather than normal brain tissues. Therefore, CD-Asp could be used as a glioma-targeting imaging agent with low toxicity to normal brain. The distributions of CD-G, CD-A, and CD-Glu in glioma are shown in Figure S11, and the result proves that CD-G and CD-Glu have much weaker targeting ability than that of CD-Asp, while CD-A has no targeting ability. Generally, transporter- and receptor-mediated transports are two major mechanisms by which various agents can cross the BBB.[47] Glucose transporter (GLUT-1) is found in high density on the BBB[48] and brain tumors,[49] conferring a brain-tumor-targeting property through facilitative glucose metabolism by the glucose transporters.[50] On the other hand, ASCT2 is an important L-isomer-selective

transporter across the BBB for L-glutamine and L-asparagine as high-affinity substrates.[51] In the present work, all these CDs prepared from glucose, L-Asp, and/or L-Glu should contain the same reactant functional groups (glucose, L-ASP, L-Glu), which help these CDs go across the BBB through the GLUT-1 and ACT2 transporters. That is why fluorescent imaging in the brain sites was observed for these CDs. As known, RGD, a tripeptide composed of L-arginine, glycine, and L-aspartic acid, is a common glioma-targeting agent that binds to $\alpha_V\beta_3$ integrin on immature endothelial cells.[52,53] Recently, Fu *et al*. reported Asp_3 also possesses a targeting function on bone cells.[54] On the other hand, glucose has been used to conjugate with photosensitizer to selectively target glioma cells of a rat model.[55,56] In our present work, we speculate about the targeting function of CD-Asp, which may originate from the formation of RGD-like functional groups on the CD's edge in the preparation of CDs from D-glucose and L-Asp. RGD-like groups result in high glioma targeting efficiency of CD-Asp. A more detailed mechanism is still under research.

In summary, CD-Asp were synthesized by a simple and facile thermolysis method with D-glucose and L-aspartic acid as starting materials. The as-synthesized CD-Asp exhibit high biocompatibility and continuous full-color emission. *In vitro* experiments indicated that CD-Asp have high selectivity and targeting ability toward C6 glioma cells. An *in vivo* imaging study further confirms that CD-Asp can localize into glioma sites with much higher intensity than normal brain tissue, indicating that CD-Asp can be used as a targeted fluorescence imaging agent of brain glioma. This work demonstrated that CDs could be used as a platform for constructing an intelligent nanomedicine with integration of diagnostic, targeting, and therapeutic functions.

Conflict of Interest: The authors declare no competing financial interest.

Supporting Information Available: The Supporting Information is available free of charge on the ACS Publications website at DOI: 10.1021/acsnano.5b05575.

Materials, general measurements, control experiments, and additional figures as described in the text (PDF)

Acknowledgment. Financial support from the National Natural Science Foundation of China (Nos. 51522307, 91227118, 21201159, and 61176016) and project support from Open Research Fund of State Key Laboratory of Polymer Physics and Chemistry are gratefully acknowledged. Z.S. thanks the support of the "Hundred Talent Program" of CAS and the Innovation and Entrepreneurship Program of Jilin. Z.X. thanks the support from a CIAC start-up fund.

REFERENCES AND NOTES

1. Agarwal, S.; Sane, R.; Oberoi, R.; Ohlfest, J. R.; Elmquist, W. F. Delivery of Molecularly Targeted Therapy to Malignant Glioma, A Disease of The Whole Brain. *Expert Rev. Mol. Med.* **2011**, *13*, e17.
2. Kobayashi, H.; Ogawa, M.; Alford, R.; Choyke, P. L.; Urano, Y. New Strategies for Fluorescent Probe Design in Medical Diagnostic Imaging. *Chem. Rev.* **2010**, *110*, 2620–2640.
3. Michalet, X.; Pinaud, F. F.; Bentolila, L. A.; Tsay, J. M.; Doose, S.; Li, J. J.; Sundaresan, G.; Wu, A. M.; Gambhir, S. S.; Weiss, S. Quantum Dots for Live Cells, *in vivo* Imaging, and Diagnostics. *Science* **2005**, *307*, 538–544.
4. Alivisatos, P. The Use of Nanocrystals in Biological Detection. *Nat. Biotechnol.* **2004**, *22*, 47–52.
5. Kairdolf, B. A.; Smith, A. M.; Stokes, T. H.; Wang, M. D.; Young, A. N.; Nie, S. Semiconductor Quantum Dots for Bioimaging and Biodiagnostic Applications. *Annu. Rev. Anal. Chem.* **2013**, *6*, 143–162.
6. Lim, E.-K.; Kim, T.; Paik, S.; Haam, S.; Huh, Y.-M.; Lee, K. Nanomaterials for Theranostics: Recent Advances and Future Challenges. *Chem. Rev.* **2015**, *115*, 327–394.
7. Yao, J.; Yang, M.; Duan, Y. Chemistry, Biology, and Medicine of Fluorescent Nanomaterials and Related Systems: New Insights into Biosensing, Bioimaging, Genomics, Diagnostics, and Therapy. *Chem. Rev.* **2014**, *114*, 6130–6178.
8. Hardman, R. A Toxicologic Review of Quantum Dots: Toxicity Depends on Physicochemical and Environmental Factors. *Environ. Health. Perspect.* **2006**, *114*, 165–172.
9. Hauck, T. S.; Anderson, R. E.; Fischer, H. C.; Newbigging, S.; Chan, W. C. *In vivo* Quantum-Dot Toxicity Assessment. *Small* **2010**, *6*, 138–144.
10. Cai, W.; Shin, D.-W.; Chen, K.; Gheysens, O.; Cao, Q.; Wang, S. X.; Gambhir, S. S.; Chen, X. Peptide-Labeled Near-Infrared Quantum Dots for Imaging Tumor Vasculature in Living Subjects. *Nano Lett.* **2006**, *6*, 669–676.
11. Selvan, S. T.; Tan, T. T.; Ying, J. Y. Robust, Non-Cytotoxic, Silica-Coated CdSe Quantum Dots with Efficient Photoluminescence. *Adv. Mater.* **2005**, *17*, 1620–1625.
12. Speranskaya, E. S.; Beloglazova, N. V.; Lenain, P.; De Saeger, S.; Wang, Z.; Zhang, S.; Hens, Z.; Knopp, D.; Niessner, R.; Potapkin, D. V.; et al. Polymer-Coated Fluorescent CdSe-Based Quantum Dots for Application in Immunoassay. *Biosens. Bioelectron.* **2014**, *53*, 225–231.
13. Baker, S. N.; Baker, G. A. Luminescent Carbon Nanodots: Emergent Nanolights. *Angew. Chem., Int. Ed.* **2010**, *49*, 6726–6744.
14. Li, H.; He, X.; Kang, Z.; Huang, H.; Liu, Y.; Liu, J.; Lian, S.; Tsang, C. H. A.; Yang, X.; Lee, S.-T. Water-Soluble Fluorescent Carbon Quantum Dots and Photocatalyst Design. *Angew. Chem., Int. Ed.* **2010**, *49*, 4430–4434.
15. Qu, D.; Zheng, M.; Du, P.; Zhou, Y.; Zhang, L.; Li, D.; Tan, H.; Zhao, Z.; Xie, Z.; Sun, Z. Highly Luminescent S, N Co-doped Graphene Quantum Dots with Broad Visible Absorption Bands for Visible Light Photocatalysts. *Nanoscale* **2013**, *5*, 12272–12277.
16. Qu, D.; Zheng, M.; Zhang, L.; Zhao, H.; Xie, Z.; Jing, X.; Haddad, R. E.; Fan, H.; Sun, Z. Formation Mechanism and Optimization of Highly Luminescent N-Doped Graphene Quantum Dots. *Sci. Rep.* **2014**, *4*, 5294.
17. Lim, S. Y.; Shen, W.; Gao, Z. Carbon Quantum Dots and Their Applications. *Chem. Soc. Rev.* **2015**, *44*, 362–381.
18. Wang, Y.; Hu, A. Carbon Quantum Dots: Synthesis, Properties and Applications. *J. Mater. Chem. C* **2014**, *2*, 6921–6929.
19. Guo, C. X.; Xie, J.; Wang, B.; Zheng, X.; Yang, H. B.; Li, C. M. A New Class of Fluorescent-Dots: Long Luminescent Lifetime Bio-Dots Self-Assembled from DNA at Low Temperatures. *Sci. Rep.* **2013**, *3*, 2957.
20. Zheng, X. T.; Ananthanarayanan, A.; Luo, K. Q.; Chen, P. Glowing Graphene Quantum Dots and Carbon Dots: Properties, Syntheses, and Biological Applications. Chen. *Small* **2015**, *11*, 1620–1635.
21. Ding, C.; Zhu, A.; Tian, Y. Functional Surface Engineering of C-Dots for Fluorescent Biosensing and *in vivo* Bioimaging. *Acc. Chem. Res.* **2014**, *47*, 20–30.
22. Sun, Y. P.; Zhou, B.; Lin, Y.; Wang, W.; Fernando, K. A. S.; Pathak, P.; Meziani, M. J.; Harruff, B. A.; Wang, X.; Wang, H.; et al. Quantum-Sized Carbon Dots for Bright and Colorful Photoluminescence. *J. Am. Chem. Soc.* **2006**, *128*, 7756–7757.
23. Yang, S. T.; Cao, L.; Luo, P. G.; Lu, F.; Wang, X.; Wang, H.; Meziani, M. J.; Liu, Y.; Qi, G.; Sun, Y. P. Carbon Dots for Optical Imaging *in vivo*. *J. Am. Chem. Soc.* **2009**, *131*, 11308–11309.

24. Huang, X.; Zhang, F.; Zhu, L.; Choi, K. Y.; Guo, N.; Guo, J.; Tackett, K.; Anilkumar, P.; Liu, G.; Quan, Q.; et al. Effect of Injection Routes on The Biodistribution, Clearance, and Tumor Uptake of Carbon Dots. *ACS Nano* **2013**, *7*, 5684–5693.
25. Zhao, Y. L.; Liu, Q.; Shakoor, S.; Gong, J. R.; Wang, D. Y. Transgenerational Safe Property of Nitrogen-Doped Graphene Quantum Dots and The Underlying Cellular Mechanismin. *Toxicol. Res.* **2015**, *4*, 270–280.
26. Liu, Q.; Guo, B.; Rao, Z. Y.; Zhang, B. H.; Gong, J. R. Strong Two-Photon-Induced Fluorescence from Photostable, Biocompatible Nitrogen-Doped Graphene Quantum Dots for Cellular and Deep-Tissue Imaging. *Nano Lett.* **2013**, *13*, 2436–2441.
27. Hong, G.; Diao, S.; Antaris, A. L.; Dai, H. Carbon Nanomaterials for Biological Imaging and Nanomedicinal Therapy. *Chem. Rev.* **2015**, 150521105328001.
28. Wang, D.; Chen, J. F.; Dai, L. Recent Advances in Graphene Quantum Dots for Fluorescence Bioimaging from Cells through Tissues to Animals. *Part. Part. Syst. Char.* **2015**, *32*, 515–523.
29. Zhu, S.; Meng, Q.; Wang, L.; Zhang, J.; Song, Y.; Jin, H.; Zhang, K.; Sun, H.; Wang, H.; Yang, B. Highly Photoluminescent Carbon Dots for Multicolor Patterning, Sensors, and Bioimaging. *Angew. Chem., Int. Ed.* **2013**, *52*, 3953–3957.
30. Song, Y.; Zhu, S.; Yang, B. Bioimaging Based on Fluorescent Carbon Dots. *RSC Adv.* **2014**, *4*, 27184–27200.
31. Tang, J.; Kong, B.; Wu, H.; Xu, M.; Wang, Y.; Wang, Y.; Zhao, D.; Zheng, G. Carbon Nanodots Featuring Efficient FRET for Real-Time Monitoring of Drug Delivery and Two-Photon Imaging. *Adv. Mater.* **2013**, *25*, 6569–6574.
32. Ge, J.; Lan, M.; Zhou, B.; Liu, W.; Guo, L.; Wang, H.; Jia, Q.; Niu, G.; Huang, X.; Zhou, H.; et al. Graphene Quantum Dot Photodynamic Therapy Agent with High Singlet Oxygen Generation. *Nat. Commun.* **2014**, *5*, 4596.
33. Wu, L.; Cai, X.; Nelson, K.; Xing, W.; Xia, J.; Zhang, R.; Stacy, A. J.; Luderer, M.; Lanza, G. M.; Wang, L. V.; et al. A Green Synthesis of Carbon Nanoparticle from Honey for Real-Time Photoacoustic Imaging. *Nano Res.* **2013**, *6*, 312–325.
34. Hsu, P. C.; Chen, P. C.; Ou, C. M.; Chang, H. Y.; Chang, H. T. Extremely High Inhibition Activity of Photoluminescent Carbon Nanodots toward Cancer Cells. *J. Mater. Chem. B* **2013**, *1*, 1774–1781.
35. Ruan, S.; Qian, J.; Shen, S.; Zhu, J.; Jiang, X.; He, Q.; Gao, H. A Simple One-Step Method to Prepare Fluorescent Carbon Dots and Their Potential Application in Non-Invasive Glioma Imaging. *Nanoscale* **2014**, *6*, 10040–10047.
36. Ruan, S.; Wan, J.; Fu, Y.; Han, K.; Li, X.; Chen, J.; Zhang, Q.; Shen, S.; He, Q.; Gao, H. Fluorescent Carbonaceous Nanodots for Noninvasive Glioma Imaging after Angiopep-2 Decoration. *Bioconjugate Chem.* **2014**, *25*, 1061–1068.
37. Yu, C.; Li, X.; Zeng, F.; Zheng, F.; Wu, S. Carbon-Dot-Based Ratiometric Fluorescent Sensor for Detecting Hydrogen Sulfide in Aqueous Media and Inside Live Cells. *Chem. Commun.* **2013**, *49*, 403–405.
38. Du, F.; Min, Y.; Zeng, F.; Yu, C.; Wu, S. A Targeted and FRET-Based Ratiometric Fluorescent Nanoprobe for Imaging Mitochondrial Hydrogen Peroxide in Living Cells. *Small* **2014**, *10*, 964–972.
39. Tao, H.; Yang, K.; Ma, Z.; Wan, J.; Zhang, Y.; Kang, Z.; Liu, Z. *In vivo* NIR Fluorescence Imaging, Biodistribution, and Toxicology of Photoluminescent Carbon Dots Produced from Carbon Nanotubes and Graphite. *Small* **2012**, *8*, 281–290.
40. Qu, D.; Sun, Z.; Zheng, M.; Li, J.; Zhang, Y.; Zhang, G. Three Colors Emission from S, N Co-doped Graphene Quantum Dots for Visible Light H_2 Production and Bioimaging. *Adv. Opt. Mater.* **2015**, *3*, 360–367.
41. Wang, Y.; Meng, Y.; Wang, S.; Li, C.; Shi, W.; Chen, J.; Wang, J.; Huang, R. Direct Solvent-Derived Polymer-Coated Nitrogen-Doped Carbon Nanodots with High Water Solubility for Targeted Fluorescence Imaging of Glioma. *Small* **2015**, *11*, 3575.
42. Zheng, M.; Liu, S.; Li, J.; Qu, D.; Zhao, H.; Guan, X.; Hu, X.; Xie, Z.; Jing, X.; Sun, Z. Integrating Oxaliplatin with Highly Luminescent Carbon Dots: An Unprecedented Theranostic Agent for Personalized Medicine. *Adv. Mater.* **2014**, *26*, 3554–3560.
43. Cao, L.; Meziani, M. J.; Sahu, S.; Sun, Y. P. Photoluminescence Properties of Graphene *versus* Other Carbon Nanomaterials. *Acc. Chem. Res.* **2013**, *46*, 171–180.
44. Shen, J.; Zhu, Y.; Yang, X.; Li, C. Graphene Quantum Dots: Emergent Nanolights for Bioimaging, Sensors, Catalysis and Photovoltaic Devices. *Chem. Commun.* **2012**, *48*, 3686–3699.
45. Li, L.; Wu, G.; Yang, G.; Peng, J.; Zhao, J.; Zhu, J. J. Focusing on Luminescent Graphene Quantum Dots: Current Status and Future Perspectives. *Nanoscale* **2013**, *5*, 4015–4039.
46. Cao, L.; Wang, X.; Meziani, M. J.; Lu, F.; Wang, H.; Luo, P. G.; Lin, Y.; Harruff, B. A.; Veca, L. M.; Murray, D. S.; et al. Carbon Dots for Multiphoton Bioimaging. *J. Am. Chem. Soc.* **2007**, *129*, 11318–11319.
47. Liu, Y.; Lu, W. Recent Advances in Brain Tumor-Targeted Nano-Drug Delivery Systems. *Expert Opin. Drug Delivery* **2012**, *9*, 671–686.
48. McAllister, M. S.; Krizanac-Bengez, L.; Macchia, F.; Naftalin, R. J.; Pedley, K. C.; Mayberg, M. R.; Marroni, M.; Leaman, S.; Stanness, K. A.; Janigro, D. Mechanisms of Glucose Transport at The Blood-Brain Barrier: an *in vitro* Study. *Brain Res.* **2001**, *904*, 20–30.
49. Luciani, A.; Olivier, J. C.; Clement, O.; Siauve, N.; Brillet, P. Y.; Bessoud, B.; Gazeau, F.; Uchegbu, I. F.; Kahn, E.; Frija, G.; et al. Glucose-Receptor MR Imaging of Tumors: Study in Mice with PEGylated Paramagnetic Niosomes. *Radiology* **2004**, *231*, 135–142.
50. Noguchi, Y.; Saito, A.; Miyagi, Y.; Yamanaka, S.; Marat, D.; Doi, C.; Yoshikawa, T.; Tsuburaya, A.; Ito, T.; Satoh, S. Suppression of Facilitative Glucose Transporter 1 mRNA Can Suppress Tumor Growth. *Cancer Lett.* **2000**, *154*, 175–182.
51. Gliddon, C. M.; Shao, Z.; LeMaistre, J. L.; Anderson, C. M. Cellular Distribution of The Neutral Amino Acid Transporter Subtype ASCT2 in Mouse Brain. *J. Neurochem.* **2009**, *108*, 372–383.
52. Chen, X.; Plasencia, C.; Hou, Y.; Neamati, N. Synthesis and Biological Evaluation of Dimeric RGD Peptide-Paclitaxel Conjugate as A Model for Integrin-Targeted Drug Delivery. *J. Med. Chem.* **2005**, *48*, 1098–1106.
53. Bibby, D. C.; Talmadge, J. E.; Dalal, M. K.; Kurz, S. G.; Chytil, K. M.; Barry, S. E.; Shand, D. G.; Steiert, M. Pharmacokinetics and Biodistribution of RGD-Targeted Doxorubicin-Loaded Nanoparticles in Tumor-Bearing Mice. *Int. J. Pharm.* **2005**, *293*, 281–90.
54. Fu, Y. C.; Fu, T. F.; Wang, H. J.; Lin, C. W.; Lee, G. H.; Wu, S. C.; Wang, C. K. Aspartic Acid-Based Modified PLGA–PEG Nanoparticles for Bone Targeting: *In vitro* and *in vivo* Evaluation. *Acta Biomater.* **2014**, *10*, 4583–4596.
55. Zhang, M.; Zhang, Z.; Blessington, D.; Li, H.; Busch, T. M.; Madrak, V.; Miles, J.; Chance, B.; Glickson, J. D.; Zheng, G. Pyropheophorbide 2-Deoxyglucosamide: A New Photosensitizer Targeting Glucose Transporters. *Bioconjugate Chem.* **2003**, *14*, 709–714.
56. Storr, T.; Merkel, M.; Song-Zhao, G. X.; Scott, L. E.; Green, D. E.; Bowen, M. L.; Thompson, K. H.; Patrick, B. O.; Schugar, H. J.; Orvig, C. Synthesis, Characterization, and Metal Coordinating Ability of Multifunctional Carbohydrate-Containing Compounds for Alzheimer's Therapy. *J. Am. Chem. Soc.* **2007**, *129*, 7453–7463.